

Journal of Materials Chemistry A

Accepted Manuscript



This is an *Accepted Manuscript*, which has been through the Royal Society of Chemistry peer review process and has been accepted for publication.

Accepted Manuscripts are published online shortly after acceptance, before technical editing, formatting and proof reading. Using this free service, authors can make their results available to the community, in citable form, before we publish the edited article. We will replace this *Accepted Manuscript* with the edited and formatted *Advance Article* as soon as it is available.

You can find more information about *Accepted Manuscripts* in the [Information for Authors](#).

Please note that technical editing may introduce minor changes to the text and/or graphics, which may alter content. The journal's standard [Terms & Conditions](#) and the [Ethical guidelines](#) still apply. In no event shall the Royal Society of Chemistry be held responsible for any errors or omissions in this *Accepted Manuscript* or any consequences arising from the use of any information it contains.

ARTICLE

Enhancing Electrical Energy Storage using Polar Polyimides with Nitrile Groups Directly Attached to the Main Chain†

Cite this: DOI: 10.1039/x0xx00000x

Imre Treufeld,^a David H. Wang,^{b,c} Brian A. Kurish,^{b,c} Loon-Seng Tan,^{b,*} Lei Zhu^{a,*}Received 00th January 2012,
Accepted 00th January 2012

DOI: 10.1039/x0xx00000x

www.rsc.org/

A set of 12 new polyimides (PIs) with one or three polar CN dipoles directly attached to the aromatic diamine part were synthesized and their electric energy storage properties were studied using broadband dielectric spectroscopy (BDS) and electric displacement-electric field (D-E) loop measurements to determine their potential for high temperature film capacitors for aerospace applications. It was found that adding highly polar nitrile groups to the PI structure increased permittivity and thus electrical energy storage, especially at high temperatures, and 3 CN dipoles were better than 1 CN dipole. Below the glass transition temperature (T_g), a weak γ transition was observed around -100 °C and a broad β transition was observed between 100-150 °C. It was the β (i.e., precursor dipolar motion before long-range segmental motion, or glass transition), rather than the γ sub- T_g transition that substantially increased the permittivity of PIs. From the BDS results on PIs having 3 nitrile groups, the enhancement in permittivity from permanent dipoles decreased with dianhydride in the order of pyromellitic dianhydride (PMDA) > 4,4'-oxydiphthalic dianhydride (OPDA) > 1,1,1,3,3,3-hexafluoropropane dianhydride (6FDA) > 4,4'-benzophenonetetracarboxylic dianhydride (BTDA). Meanwhile, the increase in permittivity also decreased in the order of para-para, meta-para, and meta-meta linkage in the diamine, suggesting that the para-para linkage favored easier dipole rotation than the meta-meta linkage. From the D-E loop study, the PIs with a combination of PMDA dianhydride and a para-para linkage exhibited the highest discharged energy density and a reasonably low loss.

1 Introduction

High dielectric constant (>5-10), high temperature (>150 °C), and low loss polymers are attractive dielectric materials for a variety of practical applications,^{1, 2} such as film capacitors for power-conditioning,³⁻⁵ power electronics in hybrid electric vehicles,⁶⁻⁸ pulsed power,⁹⁻¹¹ and gate dielectrics for field-effect transistors.^{12, 13} There have been several strategies to achieve this goal. First, a significant amount of research effort has been dedicated to converting high dielectric constant ferroelectric polymers such as poly(vinylidene fluoride) (PVDF) and its random copolymers into more or less linear dielectrics.^{14, 15} It is observed that decreasing the ferroelectric domain size to the nanoscale (i.e., nanodomains) by repeat-unit crystal isomorphism can effectively achieve the so-called relaxor ferroelectric behavior showing a narrow hysteresis loop.¹⁵ As a consequence, high dielectric constant in the range of 30-70 can be obtained with reasonably low dielectric loss. However, repeat-unit crystal isomorphism introduces defects in the crystal lattice and tends to decrease the melting temperature (T_m). For example, relaxor ferroelectric P(VDF-co-trifluoroethylene-co-1,1-chlorofluoroethylene) [P(VDF-TrFE-CFE)] and P(VDF-co-trifluoroethylene-co-chlorotrifluoroethylene) [P(VDF-TrFE-CTEF)] random terpolymers have a T_m around 125 °C, compared with the T_m s of PVDF (175 °C) and P(VDF-TrFE) (ca. 155 °C).¹⁵⁻¹⁸ Furthermore, nanosized ferroelectric domains decrease the ferroelectric-to-paraelectric (i.e., Curie) transition temperature (T_C) to around room temperature for both random terpolymers. Above room temperature, the terpolymers are in the paraelectric phase, where random dipoles highly interact with one another without any existence of ferroelectric domains. In addition to the decreased

dipolar polarization for the high temperature paraelectric phase of P(VDF-TrFE), high crystalline and amorphous dipole mobilities promote ionic and electronic mobility in the material, resulting in high dielectric losses.^{15, 19} Therefore, the challenge lies in the effort of achieving high temperature relaxor ferroelectric crystalline polymers.

The second strategy is to add permanent dipoles into a high T_g amorphous polymer matrix while avoiding the formation of ferroelectric domains. This is similar to dipolar glasses in ceramic materials,^{20, 21} and analogous to spin glasses in magnetic materials.^{22, 23} The idea is to utilize the free volume in high T_g polymers to allow relatively free rotation of individual dipoles (i.e., sub- T_g transitions²⁴) in order to enhance the dielectric constant while keeping dielectric loss low. Early work utilized nitrile-containing styrenic and acrylic amorphous polymers to achieve relatively high dielectric constant.^{25, 26} For example, poly(4-vinylbenzylcyanide) was reported to exhibit a dielectric constant as high as 7.0 at 100 kHz. Recently, polar Φ -F²⁷ and nitrile²⁸ groups were added into bisphenol A polycarbonate (PC) in order to increase its dielectric constant ($\epsilon_r = 2.95$). For example, a fluorinated tetraaryl bisphenol A PC, DiF *p*-TABPA-PC, exhibited a dielectric constant of 3.3,²⁷ and a nitrile-modified bisphenol A PC exhibited a dielectric constant of 4.0 at room temperature.²⁸

Stimulated by the above promising work, we here focus on high performance polyimides (PIs), which are attractive materials for use in highly aggressive environments because of their high T_g , mechanical toughness, and resistance to solvents, radiation, heat and oxidation.²⁹ These properties make PI films highly suitable for use in high temperature applications such as aerospace power conditioning, electronics industry, and electrical insulation materials.

Previously, Kakimoto et al. reported that attaching of nitrile pendants into PIs would enhance their dielectric constants,³⁰ and two PIs from an unsymmetrical diamine with nitrile groups showed poor solubility in aprotic solvents and only became soluble after the nitrile groups were hydrolyzed.³¹ Their dielectric properties, however, were not reported. Hybrid films based on nitrile-containing PIs/inorganic particles (pyrite ash, barium and titanium oxides) were prepared and their nano-actuation was investigated.^{32, 33} PIs containing one and two nitrile groups per repeat unit were synthesized and their piezoelectric behavior was analyzed. The polymer containing two nitrile groups per repeat unit showed higher remnant polarization than the ones containing only one nitrile group per repeat unit due to its increase in polarity. However, their values were low as compared with commercial piezoelectric polymers such as PVDF.³⁴

In this work, highly polar nitrile groups are directly attached to the aromatic diamine part of various PI structures. In total, 12 new PIs, containing 1 or 3 CN dipoles, are synthesized. Their dielectric properties and loss mechanisms are studied by broadband dielectric spectroscopy (BDS) and electric displacement-electric field (D-E) loop measurements. Results show that 3 CN dipoles are more effective than 1 CN dipole (i.e., number density effect) in enhancing the dielectric constant and thus electrical energy storage of PIs.

2 Experimental

2.1. PI synthesis and film preparation for dielectric characterization

The polyimide films were fabricated according to the previous publications.³⁵⁻³⁷ An example of PI synthesis is described in section I of the Supplementary material. The condensation polymerization of the diamines containing one or three nitrile dipoles with the dianhydrides being 2,2'-bis(3,4-dicarboxyphenyl)-1,1,1,3,3,3-hexafluoropropane dianhydride (6FDA), 4,4'-oxydiphthalic dianhydride (OPDA), 4,4'-benzophenonetetracarboxylic dianhydride (BTDA), and pyromellitic dianhydride (PMDA) was conducted in *N,N*-dimethylacetamide (DMAc) at room temperature for 24 h to afford the corresponding poly(amic acid)s (PAA), which were subsequently imidized by stepwise thermal treatment up to 300 °C to afford tough, creasable PI films (20-40 μm thickness).

Due to the polar nature, PIs tend to absorb a small amount of moisture, which may significantly affect their dielectric properties.³⁸ Therefore, all PI films were dried in a vacuum oven at 130 °C for 24 h to remove water before any dielectric property measurements. After drying, the film samples were coated with 100 nm silver electrodes on both sides by physical vapor deposition (EvoVac Deposition System, Angstrom Engineering Inc., Kitchener, Ontario, Canada) to improve electrical contact. The electrode areas were 0.785 cm² for the BDS study and 0.0515 cm² for the D-E loop study. The samples were then stored in a desiccator filled with Drierite until dielectric measurements were performed.

2.2. BDS measurements

Low-voltage BDS measurements were carried out on a Novocontrol Concept 80 broadband dielectric spectrometer (Montabaur, Germany). For temperature scans, temperature was programmed to change linearly from -150 °C to 190 °C at a rate of 2 °C/min. A sine voltage of 1.0 V_{rms} (root-mean square voltage) with frequency ranging from 10⁷ Hz to 1 Hz was applied across the sample film during temperature ramping, and data was recorded simultaneously. For frequency scans, samples were held at a constant temperature and the same sine voltage as above was applied with frequency ranging from 10⁻³ Hz to 10⁷ Hz. High-voltage (HV) BDS experiments were carried out in the same way, except that the

frequency was scanned from 10⁴ Hz to 1 Hz and the peak amplitude of the applied sinusoidal electric field was 10 and 50 MV/m.

2.3. D-E hysteresis loop measurements

D-E loop measurements were performed at 23, 100, and 190 °C, using a Premier II ferroelectric tester (Radiant Technologies, Inc., Albuquerque, New Mexico, U.S.A.). The temperature was controlled by using a clean silicone oil bath equipped with an IKA RCT temperature controller (IKA Works, Inc., Wilmington, North Carolina, U.S.A.). Two consecutive sine-wave voltages with equal amplitudes were applied to the film sample and the second loop was taken as the result to eliminate the transient effect. The frequency of each wave was fixed at 10 or 1000 Hz. Stray capacitance (i.e., background capacitance from the fixture and high voltage cables) as a function of film thickness was determined by measuring the electric displacement, *D*, of biaxially oriented polypropylene (BOPP, SB Electronics, Inc., Barre, Vermont, U.S.A.) films with different thicknesses (8-55 μm) at 4000 V. The stray capacitance was subtracted from the raw data of the film sample according to its thickness.

2.4. Density measurement

Several pieces of film samples were placed in a beaker filled with pure water and some surfactant to make sure that they sank to the bottom. After 5 min ultrasonication to remove surface bubbles, sodium iodide was gradually added until the film samples floated (or suspended) in the solution. Then, 10 mL of the solution was sampled using a pipette and weighed to determine its density. Finally, this density was taken as the sample density.

3 Results and discussion

Totally, thirteen PIs were synthesized and their dielectric properties measured. A summary of the chemical structures and the measurement results are presented in Table 1.

3.1. Effect of the number of -CN groups in the diamine part of PI

To investigate the effect of the number of nitrile groups in the diamine part of the PIs on dielectric properties, we selected three PIs from the list in Table 1. They are **1**, **2b**, and **4c**, which contain 0, 1, and 3 nitrile groups, respectively. Due to limitation of available PIs, the dianhydride part in sample **1** is different from those in samples **2b** and **4c**. Fig. 1 shows the real (ϵ_r') and imaginary (ϵ_r'') parts of relative permittivity and the dissipation factor ($\tan\delta$) as a function of temperature for samples **1**, **2b**, and **4c**. At -150 °C (see Figs. 1A, D, and G), ϵ_r' increased as the number of nitrile groups increased, from 2.93 for **1** to 3.30 for **2b**, and to 3.60 for **4c**. We shall now try to determine the origins of this increase in ϵ_r' . Even though it might seem as if the increase in ϵ_r' arises exclusively from the added nitrile groups, this has to be verified because **1**, **2b** and **4c** all have slightly different structures. At such a low temperature (-150 °C), the contribution from impurity ion migration to the relative permittivity could be ignored. Therefore, ϵ_r' itself should only originate from electronic, atomic (or vibrational), and dipolar polarizations. It is possible to accurately (usually within 1% error) predict the electronic component of the permittivity, ϵ_{re} , using the Lorentz-Lorenz relation that relates molar refraction R_M to permittivity:³⁹

$$R_M = \frac{\epsilon_{re} - 1}{\epsilon_{re} + 2} \frac{M_{RU}}{\rho} = \frac{N_A}{3\epsilon_0} \alpha_e \quad (1)$$

where M_{RU} is the molar mass of the repeat unit, ρ the bulk density of the PI, N_A the Avogadro constant, ϵ_0 the vacuum permittivity, and α_e the electronic polarizability. In this case, the molar refraction is that of the repeat unit of the PI. Molar refraction is obtained by adding up molar refractions of individual bonds (i.e., bond refractions^{39, 40})

in the repeat unit. The molar refraction for sample **1** is calculated to be $158.5 \text{ cm}^3/\text{mol}$ and the permittivity obtained for sample **1** from

Table 1 Summary of measurement results of dielectric properties of the PIs.

Group	Sample	State ^a	T _g (°C)	Density (g/cm ³)	RU density ($\times 10^{27} / \text{m}^3$)	μ_{RU} ^b (D)	Predicted P _{dip} ^c (mC/m ²)	$\Delta\epsilon_r'$ ^c (BDS)	Exp. P _{dip} ^d (mC/m ²)	P _{dip} ratio
1	6FDA-mmDAm (CP2)	Am	199	1.433	1.23	0.28	0.0056	0.054	-	-
2	a: OPDA-pmDAm(CN)	Am	255	1.367	1.39	5.32	2.27	0.635	0.36	0.16
	b: OPDA-mmDAm(CN)	Am	240	1.367	1.39	5.32	2.27	0.413	0.32	0.14
3	a: PMDA-ppDAm(CN) ₃	Cryst (high)	341	1.357	1.11	17.1	17.9	1.372	0.87	0.048
	b: PMDA-mmDAm(CN) ₃	Cryst (high)	305	1.367	1.12	17.1	18.0	0.644	0.85	0.047
4	a: OPDA-ppDAm(CN) ₃	Cryst (low)	235	1.342	0.98	16.0	13.9	1.139	0.83	0.060
	b: OPDA-mpDAm(CN) ₃	Cryst (low)	229	1.342	0.98	16.0	13.9	0.850	0.46	0.033
	c: OPDA-mmDAm(CN) ₃	Am	216	1.342	0.98	16.0	13.2	0.761	0.12	0.008
5	a: 6FDA-ppDAm(CN) ₃	Am	244	1.388	0.87	15.1	11.1	0.850	0.60	0.054
	b: 6FDA-mpDAm(CN) ₃	Am	232	1.400	0.88	15.1	11.2	0.921	0.64	0.058
	c: 6FDA-mmDAm(CN) ₃	Am	226	1.400	0.88	15.1	11.2	0.486	0.49	0.044
6	a: BTDA-ppDAm(CN) ₃	Am	238	1.357	0.98	14.1	10.9	0.583	0.49	0.045
	b: BTDA-mmDAm(CN) ₃	Am	218	1.344	0.97	14.1	10.8	0.427	0.25	0.023

^a The state of PI films was determined by X-ray diffraction (XRD), comparing the transmission- and reflection-mode XRD spectra, which are shown in section II of the Supplementary material.

^b The dipole moment of repeat unit (μ_{RU}) is calculated by the absolute value of diamine dipole moment minus dianhydride dipole moment. The dipole moments of diphenyl ether, 1,1,1,3,3,3-hexafluoropropane, benzophenone, and benzonitrile are 1.14, 2.0, 2.96, and 4.18 D, respectively.

^c $\Delta\epsilon_r'$ is the difference between the real part of relative permittivity at 190 °C and 1 kHz and that at -150 °C and 1 kHz. Since at -150 °C only electronic and atomic polarizations contribute to permittivity while at 190 °C dipole vibration also contributes, the difference of relative permittivity between the two temperatures can be attributed solely to the dipolar polarization.

^d Experimental polarization only due to dipole orientation. This is calculated as: D-E loop polarization at 190 °C and 1 kHz minus polarization from BDS at -150 °C and 100 kHz, extrapolated to a field of 100 MV/m.

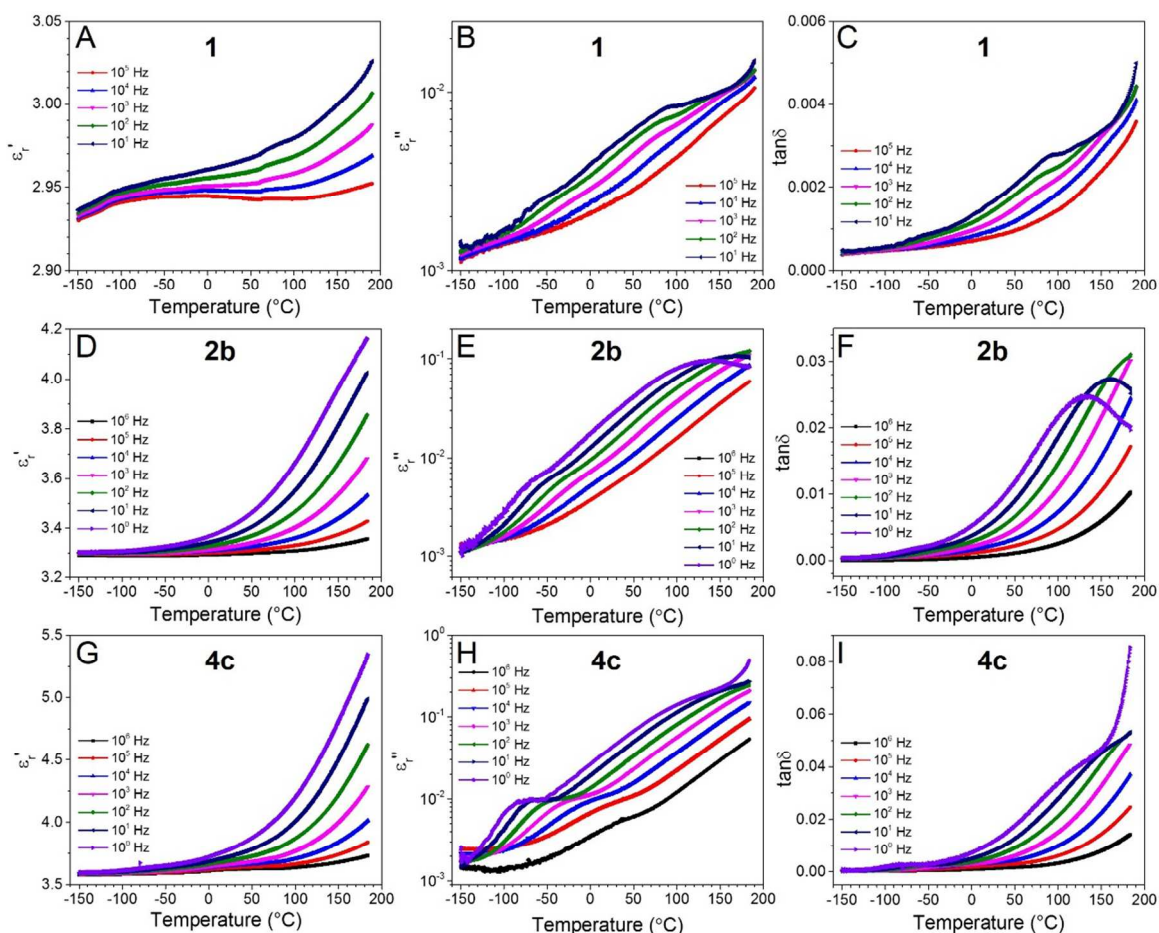


Fig. 1 ϵ_r' (A, D, G), ϵ_r'' (B, E, H), and $\tan\delta$ (C, F, I) as a function of temperature for samples **1**, **2b**, and **4c**, which contain 0, 1, and 3 -CN groups, respectively.

electronic polarization is 2.44 (see section III of the Supplementary material for calculations). This calculated value, however, is somewhat lower than the experimental value of 2.93, because it does not include vibrational and dipolar polarizations. From Fig. 1A, we can see that the contribution from dipolar polarization is insignificant, because the permittivity changes little (only 0.05 at 1 kHz) from -150 °C to 190 °C, compared with samples **2b** and **4c** which contain added nitrile groups. If we assume zero dipolar contribution to permittivity, the difference between the measured and calculated permittivity, namely 0.49, should arise from vibrational polarization for sample **1**, according to the Clausius-Mossotti relations:³⁹

$$\frac{\epsilon_r - 1}{\epsilon_r + 2} \frac{M_w}{\rho} = \frac{N_A}{3\epsilon_0} (\alpha_e + \alpha_v) \quad (2)$$

where ϵ_r has contributions from both α_e and vibrational polarizability (α_v). In other words, the magnitude of vibrational polarization is about 20% of that of the electronic polarization for sample **1**. This percentage is similar to what has been reported for polymers in general.^{39,41} Since the structures of samples **2b** and **4c** are similar to sample **1** except the nitrile groups, we assume that the percentage of vibrational polarization relative to electronic polarization is also 20% for them. Based on bond refractions,^{39,40} the molar refraction for sample **2b** is calculated to be 152.2 cm³/mol. Taking into account the 20% vibrational polarization, the permittivity ϵ_r from electronic and vibrational polarizations can be calculated to be 3.15. Comparing with the experimental ϵ_r' of 3.30, the contribution from dipolar polarization must be 0.15 for sample **2b** at -150 °C. Following the same calculation method, sample **4c** has a molar

refraction of 212.9 cm³/mol and a contribution to permittivity of 0.50 from dipolar polarization. This makes sense because **4c** has 3 CN dipoles per repeat unit as opposed to 1 CN dipole for sample **2b**, and a contribution of 0.50 from dipole motions for **4c** is approximately 3 times higher than that of 0.15 for sample **2b**. We can therefore conclude that the permittivity increase at -150 °C from sample **1** to **2b**, and finally to **4c** originates from dipolar polarization.

Upon increasing temperature from -150 °C to 190 °C, both ϵ_r' and ϵ_r'' increased for all three samples. These increases could be attributed to the enhanced dipole motion as temperature increased. Because the glass transition temperatures (T_g s) for these samples are above 200 °C (see Table 1), contribution from impurity ion migration to this increase in permittivity might be ignored for frequencies above 10 Hz. From the ϵ_r'' plots for CN-containing samples (Figs. 1 E and H), weak γ transition peaks were noticed at around -85 °C at 1 Hz. Similar relaxation peaks were also seen for other CN-containing samples (see Figs. 4, 6, and 8 later). These peaks could arise from absorbed water in the samples; although our samples had been dried in a vacuum oven at 130 °C for at least 24 h before testing, it was fairly difficult to completely eliminate trace amounts of absorbed moisture because all samples contained polar -CN groups. A similar phenomenon was also reported for Kapton, namely, a trace amount of absorbed moisture produced a relaxation peak around -100 °C.³⁸ For low frequency ϵ_r'' and $\tan\delta$ plots (Figs. 1E/F and H/I), another relatively broad relaxation peak was observed around 150-180 °C for samples **2b** and **4c** (and all other CN-containing samples; see Figs. 4, 6, and 8 later). This peak could be assigned to the β relaxation, which is often due to the onset of dipole

motions that are precursors to the long-range segmental motions in the α relaxation (or glass transition). To avoid significant deformation of samples, the upper temperature limit was chosen as 190 °C.

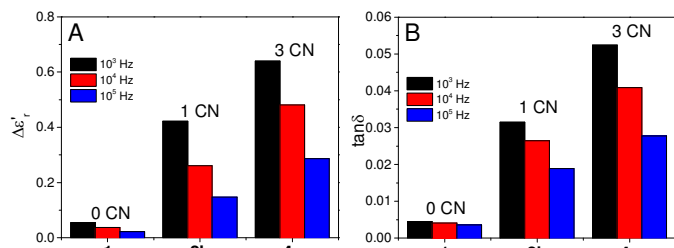


Fig. 2 (A) Increase of the real part of permittivity, $\Delta\epsilon_r'$, and (B) $\tan\delta$ at 190 °C at 10^3 , 10^4 , and 10^5 Hz for samples **1**, **2b**, and **4c**.

Fig. 2A compares the increase of ϵ_r' from -150 °C to 190 °C for samples **1**, **2b**, and **4c** at different frequencies, i.e., $\Delta\epsilon_r' = \epsilon_r'(190\text{ °C}) - \epsilon_r'(-150\text{ °C})$. Since electronic and vibrational polarizations did not change much with temperature,^{39, 42} $\Delta\epsilon_r'$ could be attributed to the change in dipolar polarization only. Clearly, adding more CN dipoles into the PI structure increased $\Delta\epsilon_r'$. For example, sample **1** did not contain any CN dipoles and its $\Delta\epsilon_r'$ was only about 0.05 at 1 kHz. Sample **2b** contained 1 CN dipole and its $\Delta\epsilon_r'$ increased to 0.41 at 1 kHz. Sample **4c** contained 3 CN dipoles and its $\Delta\epsilon_r'$ increased to 0.76 at 1 kHz.

The effect of added CN dipoles could be better understood by predicting the polarization from permanent dipoles in the sample. Assuming each repeat unit adopts an anti-parallel configuration, i.e., dianhydride and diamine dipoles orient in the opposite directions (see the chemical structures in Table 1; the dianhydride dipole moment is pointing down and the diamine dipole moment is pointing up), without external electric field, the net dipole moment of each repeat unit (μ_{RU}) can be calculated by subtracting the dianhydride dipole moment from the diamine dipole moment. According to literature, dipole moments of diphenyl ether,⁴³ 1,1,1,3,3,3-hexafluoropropane,⁴⁴ benzophenone,⁴⁵ and benzonitrile⁴⁶ are 1.14, 2.0, 2.96, and 4.18 Debyes (D), respectively. The dianhydride dipole moments increase in the order PMDA (0 D) < BTDA (14.14

D) < 6FDA (15.10 D) < OPDA (15.96 D). Samples **3a**, **4a**, **5a**, and **6a** contain these dianhydrides in this exact order (see results later), and they all have identical diamine parts, meaning that their total dipole moments would decrease from **3a** to **6a** as the dianhydride dipole moment increases. From the permittivity increase $\Delta\epsilon_r'$ from dipolar polarization (Table 1), $\Delta\epsilon_r'$ indeed decreases in the order of **3a** > **4a** > **5a** > **6a**. Therefore, it is reasonable to assume that the diamine and dianhydride parts are antiparallel in the samples.

Presently, there is no explicit theoretical prediction of dipolar polarization for main-chain polymers containing permanent dipoles, and here we resort to a freely rotating dipole model. Assuming the net dipole moment of each repeat unit, μ_{RU} , can freely rotate as a single dipole, the predicted polarization from dipole orientation (P_{dip}) is:³⁹

$$P_{dip} = N\mu_{RU} \left(\coth u - \frac{1}{u} \right), \text{ here } u = \frac{\mu_{RU}E}{k_B T} \quad (3)$$

where N is the repeat unit density, μ_{RU} the dipole moment of a repeat unit, E the applied electric field, k_B the Boltzmann constant, and T the absolute temperature. Supposedly, E should be the local electric field for the freely rotating dipole. However, there have been debates on the prediction of local field for polar materials with freely rotating permanent dipoles.⁴⁷ It is considered that the local field should be inappreciably different from the external electric field. Therefore, we use the applied electric field here. On the basis of these assumptions, the predicted polarizations from freely rotational permanent dipoles were calculated to be 0.0056, 2.27, and 13.9 mC/m² for samples **1**, **2b**, and **4c**, respectively (see Table 1). Obviously, adding more CN dipoles into PI samples increased the dipolar polarization, and thus $\Delta\epsilon_r'$ followed exactly the trend of dipolar polarization for samples **1**, **2b**, and **4c**. Nonetheless, as the permittivity increased, the dielectric loss ($\tan\delta$) at 10^3 - 10^5 Hz also increased proportionally (Fig. 2B). For polar polymers, loss mechanisms include dipole relaxation loss, impurity-ion migration loss, and electronic (or DC) conduction loss. Below, we will discuss the loss mechanisms in these PI samples.

Fig. 3 shows frequency-scan plots of ϵ_r' and ϵ_r'' for samples **1**, **2b**, and **4c** at -150 °C, 25 °C, and 190 °C. At -150 °C (Figs. 3 A and D), ϵ_r' increased with added -CN groups and remained nearly independent of frequency for all samples. Meanwhile, ϵ_r'' stayed relatively low,

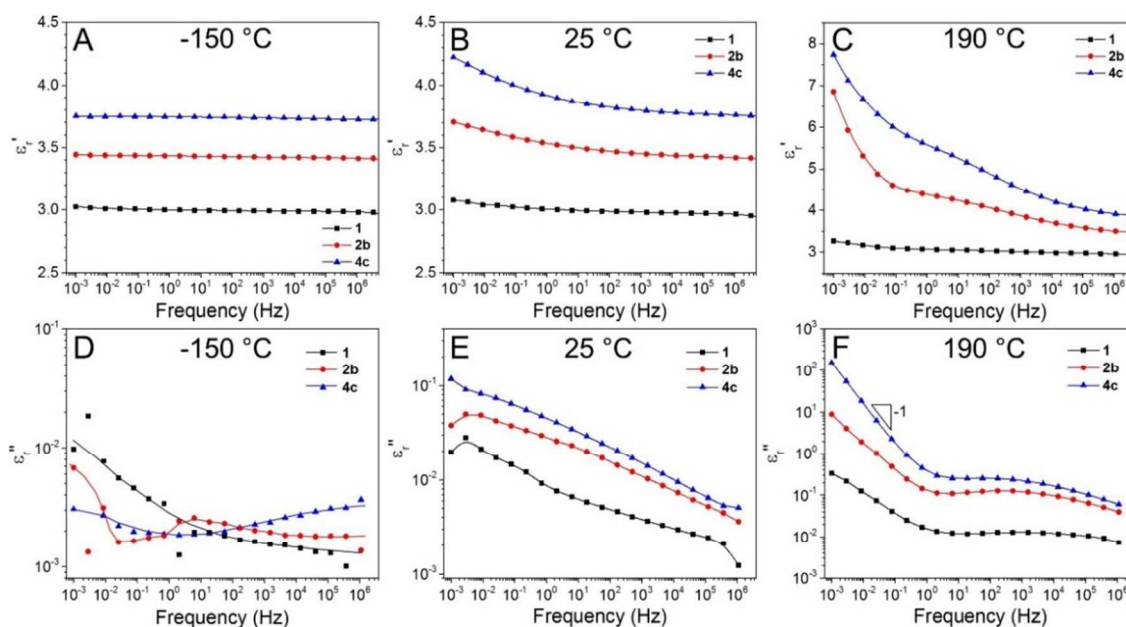


Fig. 3 Frequency-scan ϵ_r' and ϵ_r'' plots for samples **1**, **2b**, and **4c** at -150 °C (A and D), 25 °C (B and E), and 190 °C (C and F), respectively.

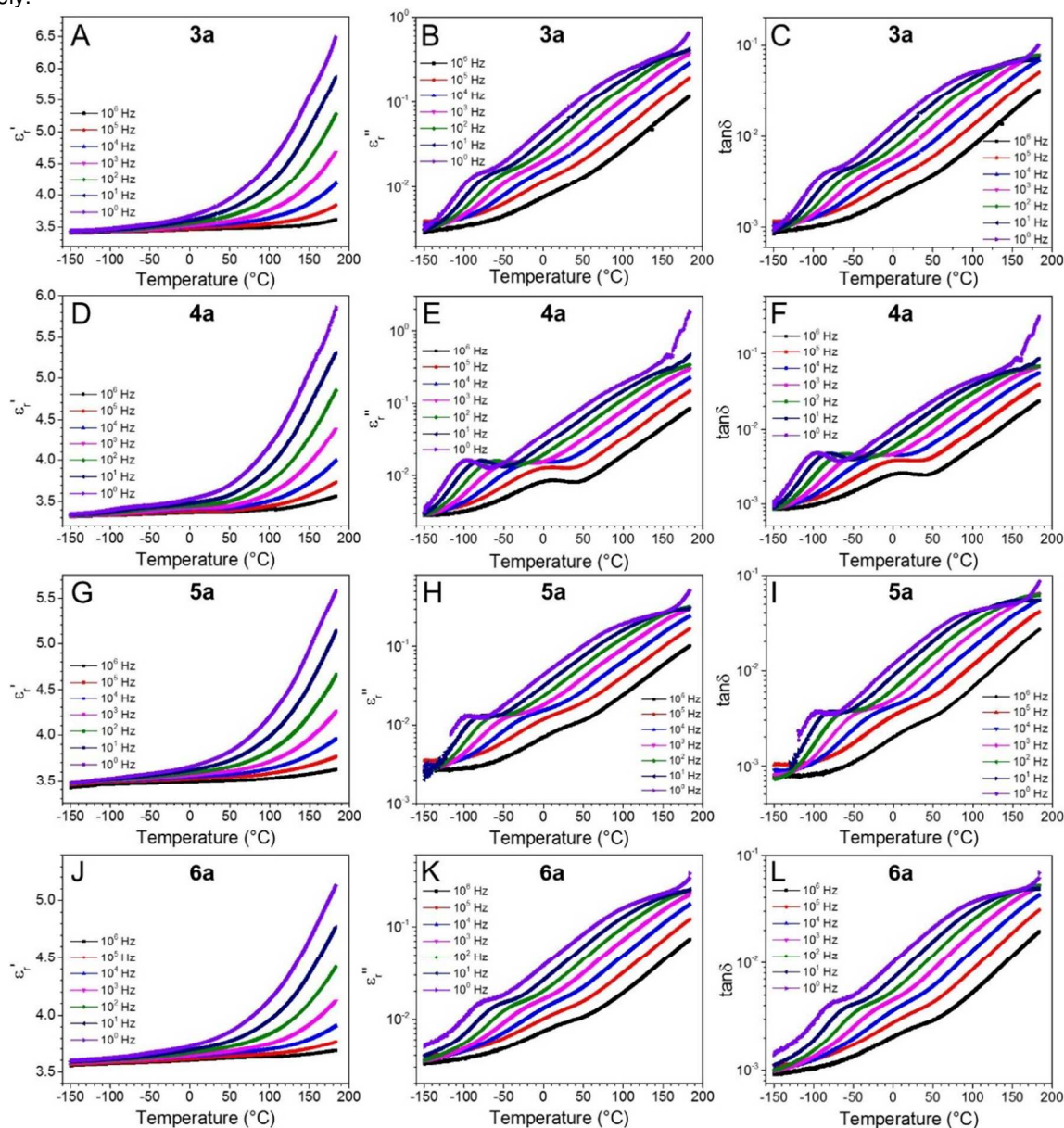


Fig. 4 Temperature-scan plots of ϵ_r' , ϵ_r'' , and $\tan\delta$ for samples **3a**, **4a**, **5a**, and **6a** with a para-para linkage in the diamine part.

between 10^{-3} and 10^{-2} (i.e., $\tan\delta$ between 3×10^{-4} and 3×10^{-3}). However, these $\tan\delta$ values were still higher than the dissipation factor for BOPP, which is around 1×10^{-5} at -150 °C.⁴⁸ At such low temperatures, both impurity-ion migration loss and electronic conduction loss could be negligible. Generally speaking, no dipole flipping should occur below the lowest sub- T_g transition temperature. However in this case, molecular motion could not be completely frozen at -150 °C and it was still possible for dipoles to wiggle even at such a low temperature, causing higher loss than in nonpolar, linear dielectric polymers such as BOPP.

Regarding sample **1** which contained no -CN dipoles, when the temperature increased from -150 °C to 25 °C and to 190 °C, there was no obvious increase in ϵ_r' at low frequencies (<1 Hz; see Figs. 3A, B, and C). This differed from samples **2b** and **4c** that contained CN dipoles. At 25 °C, ϵ_r' for samples **2b** and **4c** showed a slight increase in the low frequency region (<1 Hz), while for all samples, ϵ_r'' continuously increased with decreasing frequency, going from

0.002 to 0.03 and the loss mechanism was again primarily that from dipole motion. As the temperature increased to 190 °C, ϵ_r' for samples **2b** and **4c** had a step-wise decrease and ϵ_r'' showed a weak and broad dipole relaxation peak around 10^3 Hz with an upturn at frequencies below 1 Hz. Since the low frequency upturn has a slope close to -1, we attribute it to the impurity-ion migration loss.^{49, 50}

From the above results, we conclude that adding CN dipoles to the PI main chain primarily gives rise to two effects. First, it introduces dipolar motion (e.g. wiggling) into the PI sample. Because the -CN groups are directly attached to the main chain in a 90° configuration, this motion seems to be hindered and will cause significant friction with randomly packed neighboring chains. As a result, together with an increase in ϵ_r' , there is also an increase in ϵ_r'' due to the dipoles trying to move the main chain. This explains the trend in Fig. 2 that both ϵ_r' and ϵ_r'' increase with adding -CN groups into the PI structure. Second, by adding -CN groups, the PI samples become more polar and are easily contaminated with impurity ions with

enhanced ion mobility. At high enough temperature and low enough frequency, impurity-ion migration loss becomes significant (see Fig. 3F). For the low-field BDS spectra in Figs. 1 and 3, the applied voltage is so low (1 V_{rms}) that electronic conduction may be ignored.⁵¹

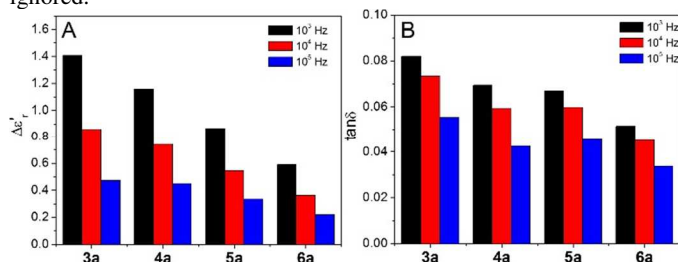


Fig. 5 (A) Increase of the real part of permittivity, $\Delta\epsilon_r'$, and (B) $\tan\delta$ at 190 °C at 10^3 , 10^4 , and 10^5 Hz for samples **3a**, **4a**, **5a**, and **6a** with a para-para linkage in the diamine.

3.2. PI samples with a para-para linkage in the diamine

From the above dielectric property measurements, we learned that PI samples with 3 nitrile groups showed high permittivity due to dipolar polarization. Below, we will focus on the PI samples containing 3 nitrile groups (see Table 1). These samples are divided into four groups based on the dianhydride part of the PI repeat unit, so each group only contains PIs with the same dianhydride part. The dianhydride parts for groups 3-6 are PMDA, OPDA, 6FDA, and BTDA, respectively. The diamine (DAm) part contains a para-para (pp), meta-para (mp), or a meta-meta (mm) linkage to the

dianhydride part. Below, we will compare dielectric properties of PI samples having the para-para linkage in the diamine part.

Fig. 4 shows temperature-scan BDS spectra for samples **3a**, **4a**, **5a**, and **6a**. For these samples, the ϵ_r' slightly fluctuated around 3.5 at -150 °C, likely due to different responses from different dianhydride parts in the samples. Upon raising the temperature from -150 °C to 190 °C, ϵ_r' showed a significant increase above ca. 50 °C. However, the amounts of increase, $\Delta\epsilon_r'$, at 10^3 , 10^4 , and 10^5 Hz are different for these samples (see Fig. 5A). Basically, $\Delta\epsilon_r'$ decreased consistently from **3a** to **6a**, which again could be attributed to the decrease of the predicted P_{dip} (see Table 1), which in turn could be associated with the rigidity of the polymer chain. For example, P_{dip} decreased from 17.9 mC/m² for **3a** to 13.9 mC/m² for **4a**, to 11.1 mC/m² for **5a**, and finally to 10.9 mC/m² for **6a**.

For samples **3a** through **6a**, γ transitions were observed around -100 °C in ϵ_r'' and $\tan\delta$ plots in Fig. 4. This could again be attributed to either dipolar group relaxation in the polymer or to the absorbed moisture. Meanwhile, a broad β relaxation shoulder peak was observed in ϵ_r'' at 1 Hz around 100-150 °C, and with increasing the frequency it moved to higher temperatures.

A comparison of $\tan\delta$ values at 10^3 - 10^5 Hz for samples **3a**-**6a** is shown in Fig. 5B. As we can see, a higher $\tan\delta$ value in Fig. 5B also coincided with a higher $\Delta\epsilon_r'$ value in Fig. 5A. From the above discussion, we understood that larger dipole motions resulted in a higher $\Delta\epsilon_r'$, which in turn also resulted in a higher $\tan\delta$, because the CN dipoles were directly attached to the PI main chain.

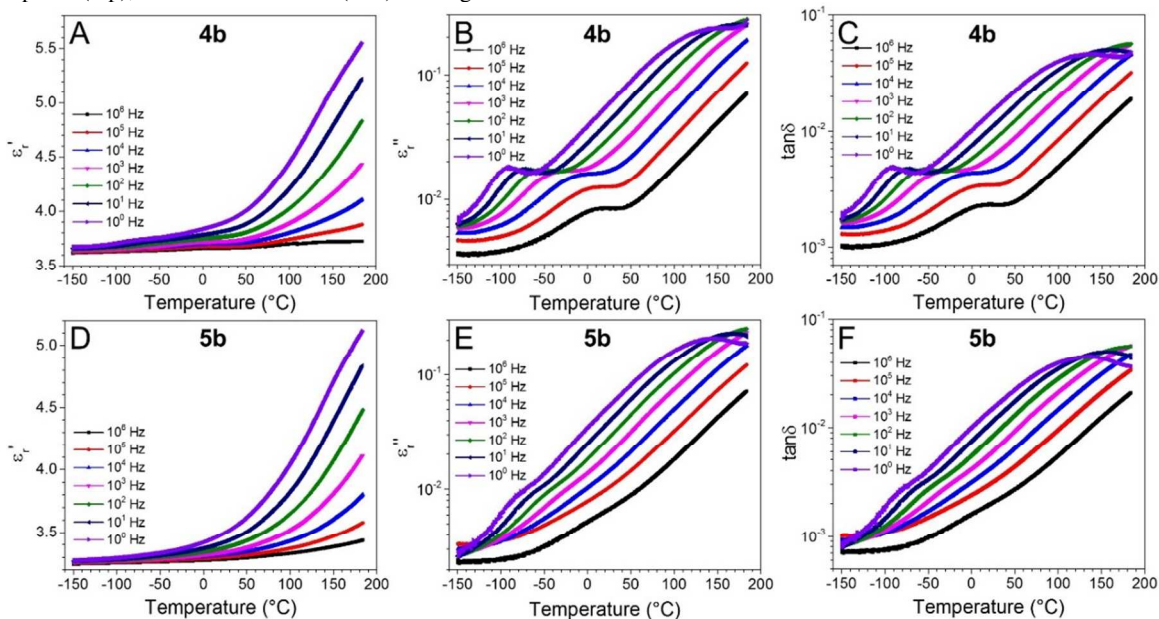


Fig. 6 Temperature-scan plots of ϵ_r' , ϵ_r'' , and $\tan\delta$ for samples **4b** and **5b** with a meta-para linkage in the diamine.

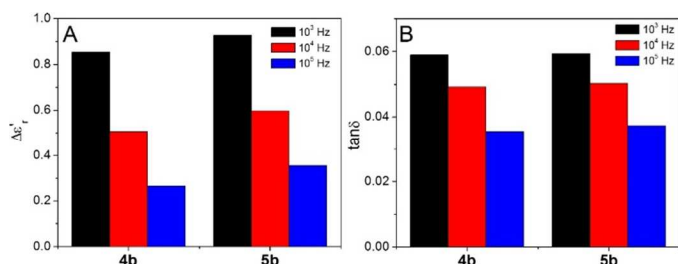


Fig. 7 (A) Increase of the real part of permittivity, $\Delta\epsilon_r'$, and (B) $\tan\delta$ at 190 °C at 10^3 , 10^4 , and 10^5 Hz for samples **4b** and **5b** with a meta-para linkage in the diamine.

3.3. PI samples with a meta-para linkage in the diamine

Fig. 6 shows the temperature-scan dielectric spectra of ϵ_r' , ϵ_r'' , and $\tan\delta$ for samples **4b** and **5b** with a meta-para linkage in the diamine. Similar results were obtained compared with the above PI samples with a para-para linkage in the diamine. At -150 °C, ϵ_r' was about 3.63 and 3.25 for samples **4b** and **5b**, respectively. With increasing the temperature up to 190 °C, ϵ_r' increased continuously. In the ϵ_r'' and $\tan\delta$ plots, the γ relaxation peak was seen at -100 °C and the β shoulder was seen at 100-150 °C at a frequency of 1 Hz. With increasing the frequency, both relaxation peaks shifted to higher

temperatures. Both $\Delta\epsilon_r'$ and $\tan\delta$ were similar for **4b** and **5b**, as shown in Fig. 7.

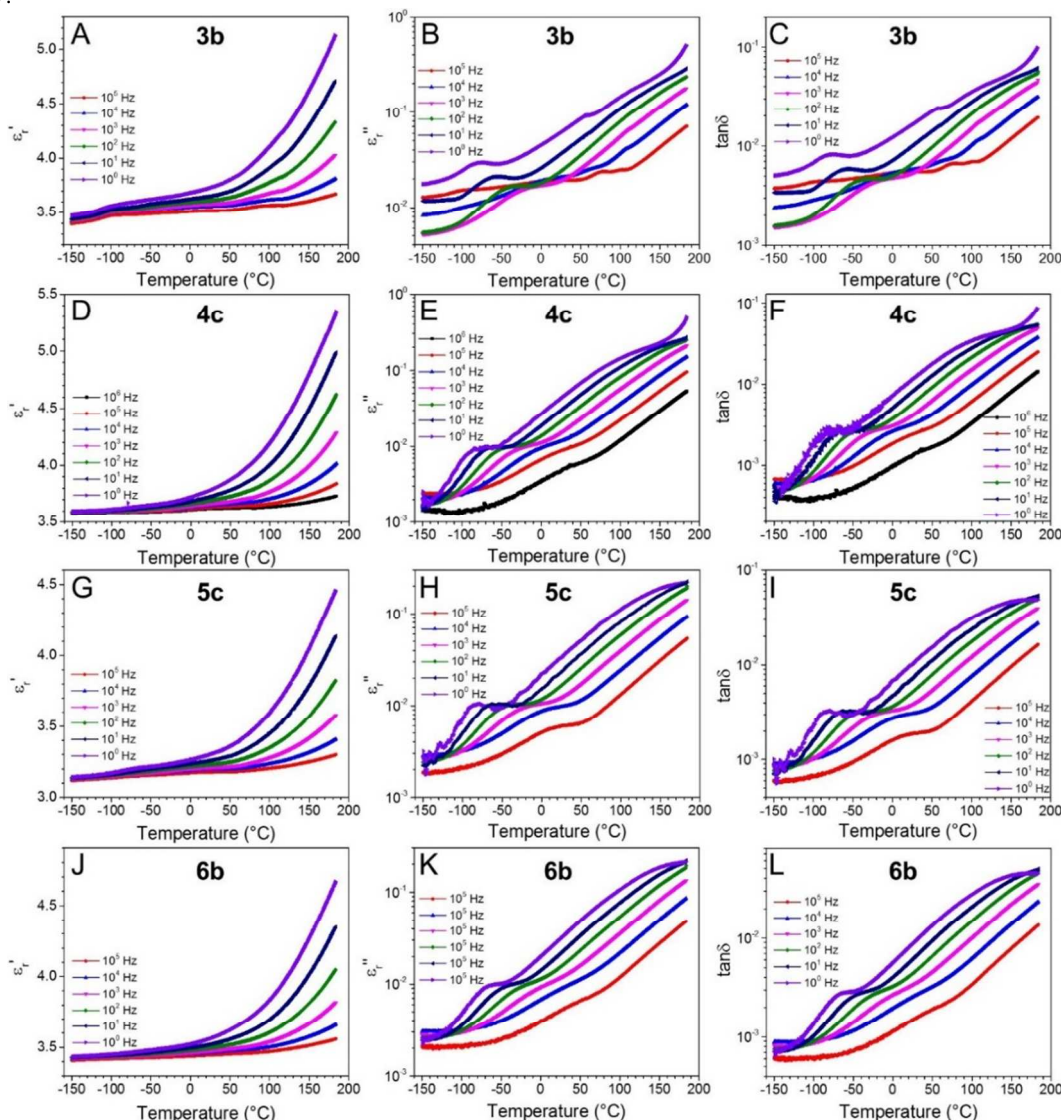


Fig. 8 Temperature-scan plots of ϵ_r' , ϵ_r'' , and $\tan\delta$ for samples **3b**, **4c**, **5c**, and **6b** with a meta-meta linkage in the diamine.

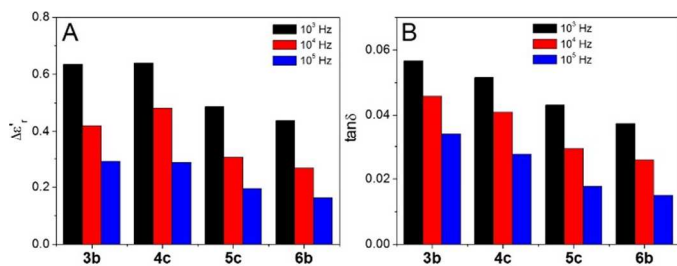


Fig. 9 (A) Increase of the real part of permittivity, $\Delta\epsilon_r'$, and (B) $\tan\delta$ at 190 °C at 10^3 , 10^4 , and 10^5 Hz for samples **3b**, **4c**, **5c**, and **6b** with a meta-meta linkage in the diamine.

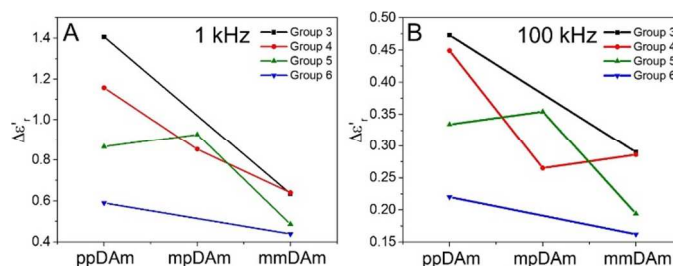


Fig. 10 Increase of the real part of permittivity, $\Delta\epsilon_r'$, at (A) 1 kHz and (B) 100 kHz for groups **3-6** with different types of linkage in diamines: para-para (ppDAm), meta-para (mpDAm), and meta-meta (mmDAm). Connecting lines are shown to guide the eye.

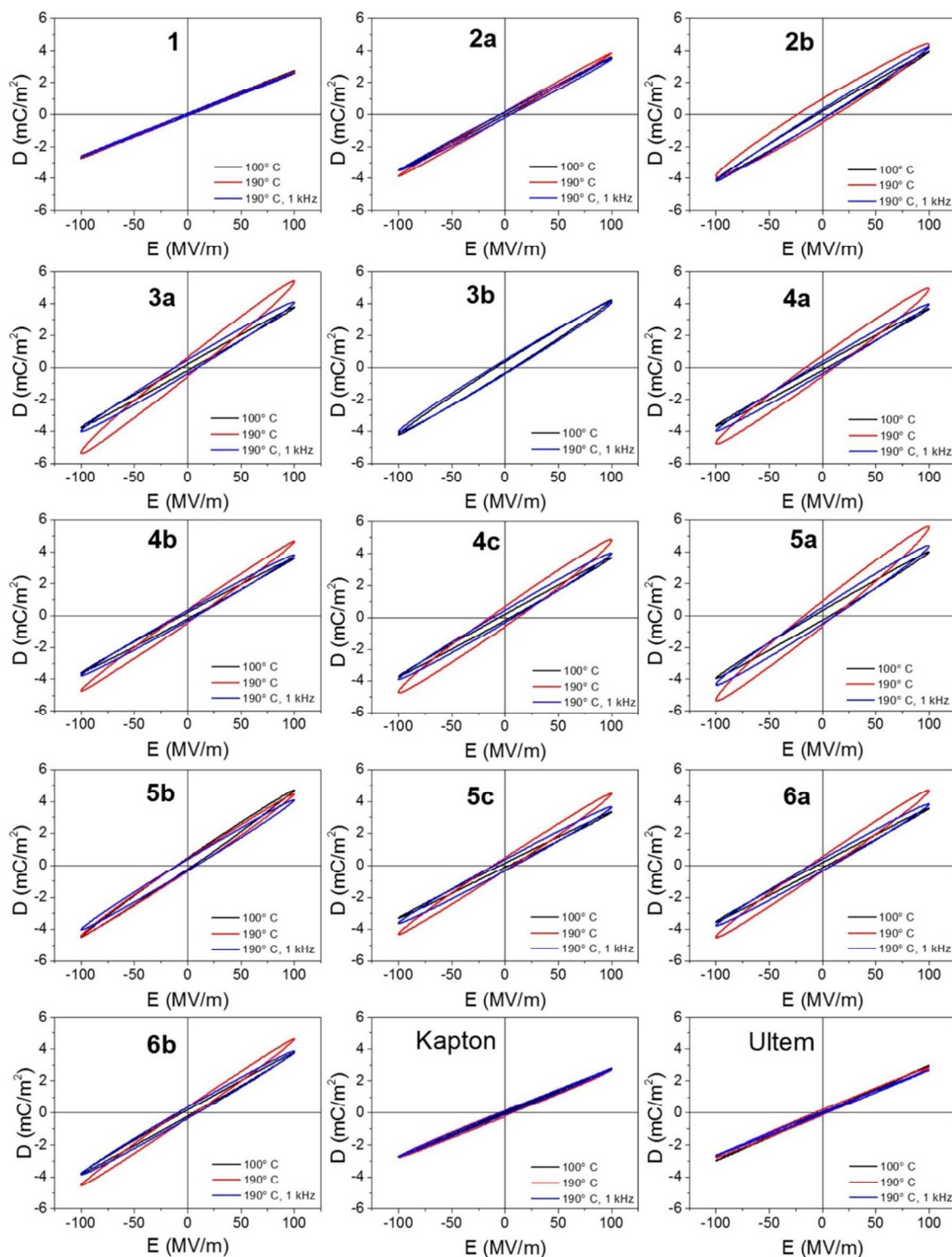


Fig. 11 Bipolar D-E hysteresis loops for various polyimide samples in Table 1, together with Kapton and Ultem, measured at 10 and 1 kHz (where noted).

ARTICLE

3.4. PI samples with a meta-meta linkage in the diamine

Fig. 8 shows the temperature-scan dielectric spectra of ϵ_r' , ϵ_r'' , and $\tan\delta$ for samples **3b**, **4c**, **5c**, and **6b** with a meta-meta linkage in the diamine. Again, similar results were obtained compared with PI samples with para-para and meta-para linkages in the diamine. The ϵ_r' values at $-150\text{ }^\circ\text{C}$ were around 3.5 for these samples, except for sample **5c**, whose ϵ_r' was ca. 3.15. With increasing temperature from $-150\text{ }^\circ\text{C}$ to $190\text{ }^\circ\text{C}$, ϵ_r' increased continuously. From the ϵ_r'' and $\tan\delta$ plots, the γ relaxation peak was seen at ca. $-80\text{ }^\circ\text{C}$ and the β shoulder was seen around $100\text{--}150\text{ }^\circ\text{C}$ for the 1 Hz curve. With increasing the frequency, both relaxation peaks shifted to higher temperatures.

Fig. 9 shows a comparison of $\Delta\epsilon_r'$ and $\tan\delta$ for samples **3b**, **4c**, **5c**, and **6b**. The $\Delta\epsilon_r'$ decreased from sample **3b** to **6b**. This was understandable because the predicted P_{dip} decreased from 18.0 mC/m^2 for **3b** to 13.2 mC/m^2 for **4c**, to 11.2 for **5c** and finally to 10.8 for **6b**. Meanwhile, $\tan\delta$ also decreased from **3b** to **6b**, because the higher predicted P_{dip} from CN dipoles directly attached to the main chain would result in a higher loss.

3.5. Effect of diamine linkage type on $\Delta\epsilon_r'$

From the above results, we learned that the dipole moment of a repeat unit played an important role in enhancing the $\Delta\epsilon_r'$. Meanwhile, we noticed that the type of linkages in the diamine also affect the $\Delta\epsilon_r'$. From Fig. 10, the general trend for groups **3-6** was that the $\Delta\epsilon_r'$ decreased from para-para to meta-para, and to meta-meta regarding the type of linkage in the diamine, regardless of whether the frequency was 1 kHz or 100 kHz. This indicates that the para-para linkage in the diamine containing 3 CN dipoles could rotate more easily than the meta-para and meta-meta linkages.

3.6. Electrical energy storage studied by D-E loops

In the above studies, we have focused on linear dielectric properties at low electric fields. In practice, polymer dielectrics are often used at high electric fields. For example, BOPP film DC-link capacitors in electric vehicles often operate at 200 MV/m and at a frequency of $10\text{--}20\text{ kHz}$.⁸ Therefore, it is highly desired to investigate high-field dielectric properties of the PI samples in Table 1. Here, we employ both D-E hysteresis loop and high-field BDS studies. Fig. 11 shows typical D-E loops under a poling field of 100 MV/m for various PI samples in Table 1, together with Kapton and Ultem for comparison. In general, one could obtain useful information on high-field dielectric properties from D-E loops. In this study, for example, the slope of the loop (i.e., $D_{\text{max}}/E_{\text{max}}$) gave the apparent dielectric constant; the charged and discharged energy densities (U_e) were obtained from $U_e = \int E dD$ of the respective charging and discharging curves;^{52, 53} the loop area represented the energy lost. The loss mechanisms again include electronic conduction, impurity ion migration, and dipole motion. From a recent report,⁵⁴ we understand that electronic conduction shifts up the upper half of the D-E loop, and impurity ionic migration and dipole switching broaden the loop symmetrically and increase the slope as well. Therefore, the loss from electronic conduction can be deconvoluted. However, it is fairly difficult to deconvolute contributions from impurity ions and dipoles in one D-E loop. One way to circumvent this difficulty is to run D-E loops at a high enough frequency (e.g., 1 kHz or above) so that the contribution

from impurity ion migration could be minimized, because relaxation for amorphous dipoles usually occurs above 1 kHz whereas impurity ions in polymers are often slow, e.g., below 1 kHz. Examples of dipolar and impurity ion losses have been discussed in Figs. 3C and F.

From Fig. 11, PI samples without any CN dipoles, such as **1**, Kapton, and Ultem, exhibited narrow loops, no matter what the frequencies and temperatures. This is the advantage of linear dielectric polymers. On the other hand, PI samples with CN dipoles exhibited broader loops. Below, we will discuss the different loss mechanisms for CN-containing PI samples. Careful inspection of D-E loops for CN-containing PI samples indicated that electronic conduction loss was not a significant loss mechanism for the PI samples because most loops (except that of **2b**, which may result from defects such as pin-holes in the sample) were symmetrical about the electric field axis. We consider that electron traps in these PI samples were effective in preventing the hopping mechanism of electron conduction⁵⁵ when the temperature was below the T_g . At $100\text{ }^\circ\text{C}$, all D-E loops at the poling frequency of 10 Hz appeared relatively narrow, indicating that electron traps were effective at a temperature at least $100\text{ }^\circ\text{C}$ below the T_g . At $190\text{ }^\circ\text{C}$ and 1 kHz, the D-E loops appeared slightly broader than those at $100\text{ }^\circ\text{C}$ and 10 Hz. Considering the dipole relaxation peak at $190\text{ }^\circ\text{C}$ around 1 kHz (Fig. 3F), the loss mechanism at $190\text{ }^\circ\text{C}$ and 1 kHz should be attributed to dipole wiggling in the CN-containing PI samples. However, the loops measured at $190\text{ }^\circ\text{C}$ and 10 Hz (shown in red) had a steeper slope than those measured at $190\text{ }^\circ\text{C}$ and 1 kHz. This could be attributed to additional impurity ion migration in the samples because migration of impurity ions increases the loss (i.e., broader loops) and the accumulation of these ions at both electrodes increases the capacitance and thus the slope of the D-E loops.⁵⁴ On the basis of our previous reports, less than ppm level of impurity ions could cause significant impurity-ion migration loss.⁵¹

To understand the effect of dipolar polarization, we had to exclude the loss mechanism due to impurity ions. As we mentioned above, running D-E loops at 1 kHz could possibly eliminate the influence from impurity ions because their motion is slower than that of dipoles. From the D-E loops at $190\text{ }^\circ\text{C}$ and 1 kHz, an apparent dielectric constant could be obtained. If we assume that the permittivity at $-150\text{ }^\circ\text{C}$ and 100 kHz in the BDS study originated solely from deformational (i.e., electronic and vibrational) polarization, the polarization from dipoles could be obtained from the difference between the D-E loop apparent dielectric constant at $190\text{ }^\circ\text{C}$ and 1 kHz and the BDS permittivity at $-150\text{ }^\circ\text{C}$ and 100 kHz. Table 1 lists the experimental P_{dip} values for different PI samples. The ratio between experimental P_{dip} and predicted P_{dip} could be an indicator of dipole wiggling in the PI samples at $190\text{ }^\circ\text{C}$. For samples containing 1 nitrile group, the ratio was about 0.15, whereas for samples containing 3 nitrile groups, the ratio was only around 0.05. This suggested that fixing CN dipoles onto rigid PI main chains significantly decreased their mobility, compared with the freely rotating model (see Eqn. 3). In addition, introducing more CN dipoles onto the PI main chain further increased the polymer rigidity.

The discharged energy densities and loss% at an applied field of 100 MV/m were obtained from D-E loops for all samples, and results are summarized in Figs. 12 and 13. Samples **3a** and **3b**

exhibited the highest discharged energy density with reasonably low loss%.

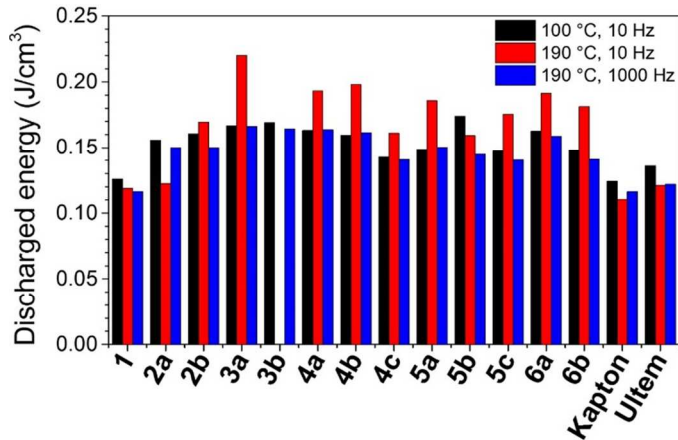


Fig. 12 Discharged energy density of different PIs from D-E loop measurements at 100 MV/m at different temperatures and frequencies.

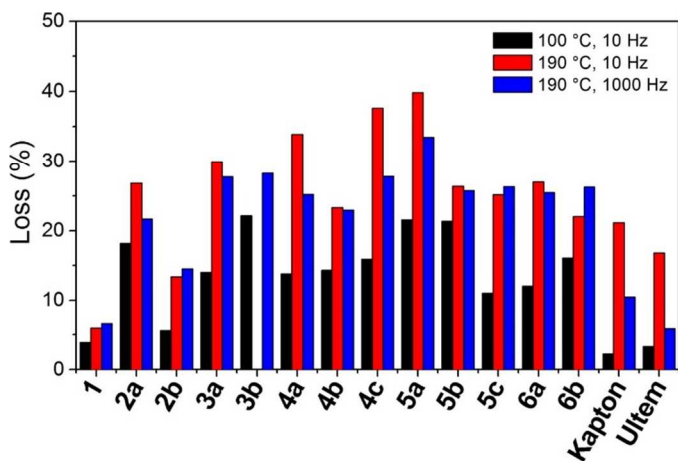


Fig. 13 Hysteresis loop loss% from D-E loop measurements at 100 MV/m at different temperatures and frequencies for different PI samples.

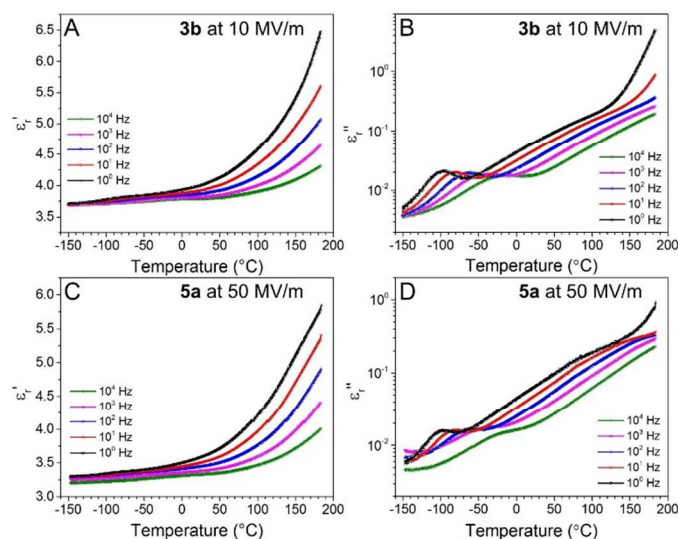


Fig. 14 ϵ_r' and ϵ_r'' versus temperature for samples **3b** and **5a** under a high electric field with a peak amplitude of 10 MV/m for **3b** and 50 MV/m, for **5a**.

PI samples without any nitrile groups had the lowest loss%; however, their discharged energy densities were also the lowest. For example, the discharged energy density for **3a** at 190 °C and 10 Hz was about 1.9 times those for samples **1**, Kapton, and Ultem (see Fig. 12). From Fig. 13, the closer the heights of the red (190 °C and 10 Hz) and blue (190 °C and 1 kHz) bars, the less ionic and electronic conduction loss because the loss% at 190 °C and 10 Hz included losses from impurity ion migration and dipole motion, whereas the loss% at 190 °C and 1 kHz should be exclusively due to dipole motion.

3.7. High voltage BDS study

In addition to D-E loops, high-field dielectric properties were also studied using HV BDS, and the results for samples **3b** and **5a** are shown in Fig. 14. These results look similar to the low-field BDS spectra; however, there are differences. First, the ϵ_r' values at -150 °C for both samples were around 3.5 and increased with increasing temperature. The difference was that the $\Delta\epsilon_r'$ at 1 kHz was higher for HV BDS than for normal BDS. For example, $\Delta\epsilon_r'$ was 1.25 and 1.06 in HV BDS, whereas it was 0.62 and 0.87 in low-field BDS for samples **3b** and **5a**, respectively. Second, γ and β relaxation peaks were also observed in HV BDS ϵ_r'' plots for samples **3b** and **5a**. However, the ϵ_r'' values were much higher in HV BDS than those in low-field BDS. This could be attributed to enhanced electronic conduction, impurity ion migration, and dipole motion under high electric fields.

As we can see from Table 1, the fraction of dipole flipping for most of the samples is only about 0.05. This can be explained by the rigid structure of the PIs, which does not allow dipoles to turn. This rigid structure of course is what imparts PIs their great thermal stability. Also, from Fig. 2B, dielectric losses increase with the addition of CN dipoles. Since the CN dipoles are attached to the main chain of the PIs in all samples studied, the chain needs to turn with the CN dipoles when an electric field is applied. The result is obvious: the dipoles are difficult to turn because they need to turn part of the rigid main chain. However, small amplitude turning may still occur, but is hampered by strong friction forces giving rise to relatively high losses. To solve this problem of low dipole turning and high loss, the dipoles should not be attached directly to the PI main chain. Bendler et al.²⁸ reported a study attaching cyanomethylene groups to bisphenol A polycarbonate (PC), having a CH₂ group between the main chain and the nitrile group so that the dipole could rotate more freely in the side group. The CN-modified PC achieved a polarization fraction of 0.10 of the theoretical prediction and a dielectric constant of 4.0. In the future, we plan to attach -CH₂CN groups to PIs in order to enhance the dipole mobility but keep the dipolar loss low.

4. Conclusions

In this work, we systematically investigated a series of PI samples containing highly polar nitrile groups. BDS and D-E loop results indicated that adding CN dipoles into PI structures increased the permittivity. Especially on the diamine unit basis, 3 nitrile groups were more effective than 1 nitrile group in increasing the permittivity. Among polar PI samples having 3 nitrile groups, the dipole moment of the dianhydride also played an important role. With increasing the dipole moment of the dianhydride part in the order of PMDA, OPDA, 6FDA, and BTDA, the enhancement of permittivity gradually decreased. This suggested that the dianhydride and diamine should arrange in an opposite direction with dipole moments cancelling each other on the molecular scale. In addition, para-para linkage in the diamine yielded a higher

permittivity than meta-para and meta-meta linkages between dianhydride and diamine parts due to easier rotation around the para-para bonds. From the high-field D-E loop study, discharged energy density and loss% were obtained. Sample **3a** exhibited the highest discharged energy density due to its high dipolar polarization. From the HV BDS study, even higher permittivities were observed.

Although enhanced permittivity was achieved for these CN-containing PI samples, dielectric losses, i.e., $\tan\delta$ and loss%, were also increased. This could be attributed to the fact that CN dipoles were directly attached to the PI main chain. In a recent study,²⁸ the nitrile group was attached to the bisphenol-A unit of PC via a methylene group. The rotation of the acetonitrile side group became easier than the nitrilephenyl main chain in our PI samples. In the future, we will synthesize PI samples with a polarizable side group such as $-\text{CH}_2\text{CN}$ in order to achieve higher permittivity and electrical energy storage while maintaining a low dielectric loss.

Acknowledgements

The authors acknowledge AFRL Materials and Manufacturing Directorate for partial financial support. We thank Zhongbo Zhang for performing the reflection-mode XRD measurements and Michelle Song for helping with the D-E loop measurements. We are also grateful for helpful discussion with Dr. Elshad Allahyarov and Professor Donald Schuele at Case Western Reserve University. IT is grateful to the U.S. Department of State for the International Fulbright Science and Technology Award.

Notes and references

^a Department of Macromolecular Science and Engineering and Department of Chemistry, Case Western Reserve University, Cleveland, Ohio 44106-7202, U.S.A.

^b Air Force Research Laboratory, Materials and Manufacturing Directorate, Nanostructured and Biological Materials Branch, Wright-Patterson Air Force Base, OH 45433, U.S.A.

^c UES, Inc., Dayton, OH 45432, U.S.A.

† Electronic Supplementary Information (ESI) available: Syntheses of monomers and polymers, reflection and transmission X-ray diffraction profiles, details of calculation, and BDS results for sample **2a**. See DOI: 10.1039/b000000x/

- W. J. Sarjeant, J. Zirnheld and F. W. MacDougall, *IEEE Trans. Plasm. Sci.*, 1998, **26**, 1368-1392.
- Q. Tan, P. Irwin and Y. Cao, *IEEJ Trans. Fund. Mater.*, 2006, *126*, 1152-1159.
- N. Venkat, T. D. Dang, Z. W. Bai, V. K. McNier, J. N. DeCerro, B. H. Tsao and J. T. Stricker, *Mater. Sci. Eng. B*, 2010, **168**, 16-21.
- J. Ho and T. R. Jow, *Characterization of High Temperature Polymer Thin Films for Power Conditioning Capacitors*, Army Research Laboratory, Adelphi, MD, 2009.
- W. J. Sarjeant, I. W. Clelland and R. A. Price, *P. IEEE*, 2001, **89**, 846-855.
- H. Wen, W. Xiao, X. Wen and P. Armstrong, *IEEE Trans. Veh. Technol.*, 2012, **61**, 2950-2964.
- C. Zou, Q. M. Zhang, S. H. Zhang, D. Kushner, X. Zhou, R. Bernard and R. J. Orchard, *J. Vac. Sci. Technol. B*, 2011, **29**, 061401.
- D. Montanari, K. Saarinen, F. Scagliarini, D. Zeidler, M. Niskala and C. Nender, *Film Capacitors for Automotive and Industrial Applications*. 2009 CARTS Proceedings, April 2009, Jacksonville, FL, U.S.A.
- S. H. Zhang, B. Zellers, J. Henrich, S. Rockey, D. Anderson, C. Zou and Q. M. Zhang, *High Energy Density Film Capacitors. 2009 IEEE Pulsed Power Conference*, Vols. 1 and 2, 2009, 776-780.
- Y. Wang, X. Zhou, Q. Chen, B. Chu and Q. M. Zhang, *IEEE Trans. Dielectr. Electr. Insul.*, 2010, **17**, 1036-1042.
- F. MacDougall, J. Ennis, X. H. Yang, K. Seal, S. Phatak, B. Spinks, N. Keller, C. Naruo and T. R. Jow, *Large High Energy Density Pulse Discharge Capacitor Characterization*. 2005 IEEE International Pulsed Power Conference, Monterey, CA, 2005, 1215-1218.
- A. Facchetti, M. H. Yoon and T. J. Marks, *Adv. Mater.*, 2005, **17**, 1705-1725.
- J. Veres, S. Ogier, G. Lloyd and D. de Leeuw, *Chem. Mater.*, 2004, **16**, 4543-4555.
- L. Zhu and Q. Wang, *Macromolecules*, 2012, **45**, 2937-2954.
- L. Yang, X. Li, E. Allahyarov, P. L. Taylor, Q. M. Zhang and L. Zhu, *Polymer*, 2013, **54**, 1709-1728.
- T. C. Chung and A. Petchsuk, *Macromolecules*, 2002, **35**, 7678-7684.
- Y. Lu, J. Claude, B. Neese, Q. Zhang and Q. Wang, *J. Am. Chem. Soc.*, 2006, **128**, 8120-8121.
- Y. Lu, J. Claude, L. E. Norena-Franco and Q. Wang, *J. Phys. Chem. B*, 2008, **112**, 10411-10416.
- R. Su, J. K. Tseng, M. S. Lu, M. Lin, Q. Fu and L. Zhu, *Polymer*, 2012, **53**, 728-739.
- G. A. Samara, *J. Phys.: Condens. Matter*, 2003, **15**, R367-R411.
- A. A. Bokov and Z. G. Ye, *J. Mater. Sci.*, 2006, **41**, 31-52.
- J. L. Dormann, D. Fiorani and E. Tronc, *Adv. Chem. Phys.*, 1997, **98**, 283-494.
- D. L. Leslie-Pelecky and R. D. Rieke, *Chem. Mater.*, 1996, **8**, 1770-1783.
- J. R. Fried, in *Physical Properties of Polymers Handbook*, Springer, New York, 2007, Chapter 13, 217-232.
- F. Bai, T. D. Jones, T. W. Kelley, T.-C. Lee, K. M. Lewandowski and D. V. Muryes, *Organic polymers, electronic devices, and methods. U.S. Patent*, US2004/0222415, November 11, 2004.
- F. Bai, T. D. Jones, T. W. Kelley, T.-C. Lee, K. M. Lewandowski and D. V. Muryes, *Organic polymers, laminates, and capacitors. U.S. Patent*, US2005/0019592 A1, January 27, 2005.
- J. T. Bendler, C. A. Edmondson, M. C. Wintersgill, D. A. Boyles, T. S. Filipova and J. J. Fontanella, *Eur. Polym. J.*, 2012, **48**, 830-840.
- J. T. Bendler, D. A. Boyles, C. A. Edmondson, T. Filipova, J. J. Fontanella, M. A. Westgate and M. C. Wintersgill, *Macromolecules*, 2013, **46**, 4024-4033.
- M. K. Ghosh and K. L. Mittal, *Polyimides: Fundamentals and Applications*, Marcel Dekker, New York, 1996.
- L. Li, R. Kikuchi, M. A. Kakimoto, M. Jikei and A. Takahashi, *High Perform. Polym.*, 2005, **17**, 135-147.
- H. A. Kang, I. S. Chung, M. A. Kakimoto and S. Y. Kim, *Polym. J.*, 2001, **33**, 284-289.
- C. Hamciuc, E. Hamciuc, M. Ignat and G. Zarnescu, *High Perform. Polym.*, 2009, **21**, 205-218.
- E. Hamciuc, C. Hamciuc and M. Ignat, *High Perform. Polym.*, 2010, **22**, 225-236.
- B. Gonzalo, J. L. Vilas, T. Brezczewski, M. A. Perez-Jubindo, M. R. De La Fuente, M. Rodriguez and L. M. Leon, *J. Polym. Sci., Part A: Polym. Chem.*, 2009, **47**, 722-730.
- J. D. Jacobs, M. J. Arlen, D. H. Wang, Z. Ounaies, R. Berry, L. S. Tan, P. H. Garrett and R. A. Vaia, *Polymer*, 2010, **51**, 3139-3146.
- D. H. Wang, J. K. Riley, S. P. Fillery, M. F. Durstock, R. A. Vaia and L. S. Tan, *J. Polym. Sci., Part A: Polym. Chem.*, 2013, **51**, 4998-5011.
- D. H. Wang, B. A. Kurish, I. Treufeld, L. Zhu and L.-S. Tan, *J. Polym. Sci., Part A: Polym. Chem.*, 2014, submitted.
- J. Melcher, Y. Daben and G. Arlt, *IEEE Trans. Electr. Insul.*, 1989, **24**, 31-38.
- A. R. Blythe and D. Bloor, *Electrical Properties of Polymers*, 2nd edn., Cambridge University Press, New York, 2005.
- A. I. Vogel, W. T. Cresswell, G. H. Jeffery and J. Leicester, *J. Chem. Soc.*, 1952, 514-549.
- S. Millefiori, A. Alparone, A. Millefiori and A. Vanella, *Biophys. Chem.*, 2008, **132**, 139-147.
- M. A. Buldakov, I. I. Matrosov and V. N. Cherepanov, *Opt. Spectrosc.*, 2000, **89**, 37-41.
- I. E. Coop and L. E. Sutton, *J. Chem. Soc.*, 1938, 1869-1872.
- A. R. H. Goodwin and J. B. Mehl, *Int. J. Thermophys.*, 1997, **18**, 795-806.
- C. W. N. Cumper and A. P. Thurston, *J. Chem. Soc. Perkin Trans. 2*, 1972, 106-111.
- K. Wohlfart, M. Schnell, J. U. Grabow and J. Kupper, *J. Mol. Spectrosc.*, 2008, **247**, 119-121.
- J. S. Blakemore, *Solid State Physics*, 2nd edn., Cambridge University Press, New York, 1985.
- A. Kahouli, O. Gallot-Lavallee, P. Rain, O. Lesaint, C. Guillermin and J.-M. Lupin, *Relationship between structure and dielectric properties of*

- bi-oriented isotactic polypropylene films for capacitors. 2013 IEEE International Conference on Solid Dielectrics, Bologna, 2013, 1068-1071.
49. F. Kremer and A. Schönhal, *Broadband Dielectric Spectroscopy*, Springer, New York, 2003.
 50. L. F. Chen, *Microwave Electronics: Measurement and Materials Characterization*, Wiley, Hoboken, NJ, 2004.
 51. M. Mackey, D. E. Schuele, L. Zhu and E. Baer, *J. Appl. Phys.*, 2012, **111**, 113702.
 52. F. Guan, J. Wang, L. Yang, J. K. Tseng, K. Han, Q. Wang and L. Zhu, *Macromolecules*, 2011, **44**, 2190-2199.
 53. B. Chu, X. Zhou, K. Ren, B. Neese, M. R. Lin, Q. Wang, F. Bauer and Q. M. Zhang, *Science*, 2006, **313**, 334-336.
 54. L. Yang, E. Allahyarov, F. Guan and L. Zhu, *Macromolecules*, 2013, **46**, 9698-9711.
 55. K.-C. Kao, *Dielectric Phenomena in Solids: with Emphasis on Physical Concepts of Electronic Processes*, Elsevier Academic Press, Boston, 2004.